MDPI

Article

Role of the Dilution of the Gd Sublattice in Forming the Scintillation Properties of Quaternary (Gd,Lu)$_3$Al$_2$Ga$_3$O$_{12}$: Ce Ceramics

Mikhail Korzhik [1,2,*], Vasilii Retivov [2,3], Alexei Bondarau [1], Georgiy Dosovitskiy [3], Valery Dubov [2,3], Irina Kamenskikh [4], Petr Karpuk [2,3], Daria Kuznetsova [2,3], Valentina Smyslova [2,3], Vitaly Mechinsky [1,2], Vladimir Pustovarov [5], Dmitry Tavrunov [5], Evgeniy Tishchenko [4] and Andrei Vasil'ev [6]

[1] Institute for Nuclear Problems, Belarus State University, 11 Bobruiskaya, 220030 Minsk, Belarus
[2] National Research Center "Kurchatov Institute", 123098 Moscow, Russia
[3] NRC "Kurchatov Institute"—IREA, 107076 Moscow, Russia
[4] Physical Department of Moscow State University, 119991 Moscow, Russia
[5] Physics Department, Ural Federal University, 620002 Yekaterinburg, Russia
[6] Skobelchin Institute for Nuclear Physics, Moscow State University, 119991 Moscow, Russia
* Correspondence: mikhail.korjik@cern.ch

Abstract: Technological factors and processes contributing to the scintillation mechanism have been considered in quaternary garnet ceramics doped with Ce(Gd,Lu)$_3$Al$_2$Ga$_3$O$_{12}$. The super-stoichiometric additive of gadolinium in the material composition or its co-doping with a low concentration of Mg were found to be effective tools to suppress phosphorescence in the quaternary garnet, confirming that it is not an intrinsic property of the material. The Monte-Carlo simulation of electronic excitation transfer demonstrates that the hopping migration along the gadolinium sublattice plays an essential role in forming the scintillation kinetic parameters. Breaking the integrity of the gadolinium sublattice by substitution with heavier lutetium ions increases the role of self-trapped states in the excitation of Ce^{3+} ions, which ensures both an increase in the fraction of short ~20 ns and very long ~600 ns components in the scintillation kinetics.

Keywords: scintillation; cerium; lutetium; quaternary garnet; light yield; decay time; phosphorescence

1. Introduction

Scintillation materials used for the detection of different kinds of ionizing radiation demonstrate a spectacular improvement in their operational parameters when compositional disorder is introduced either in the cationic or anionic subsystem [1,2]. In particular, this progress is seen when transferring from binary to ternary compounds with a garnet structure [3]. In line with this research, large-diameter Gd$_3$Al$_2$Ga$_3$O$_{12}$:Ce (GAGG:Ce) single crystals were grown a few years ago by the Czochralski method and exhibited a higher light yield (LY) of 46,000 ph/MeV [4]. A partial substitution of Gd with Y in the composition makes the crystal quaternary, which reveals an even better LY of ~50,000 ph/MeV and faster scintillation kinetics as well [5]. The incorporation of Gd in the composition of multi-cationic garnets for brighter scintillation is preferable due to the capability of the Gd sublattice in the crystal to be a reservoir for Frenkel-type excitons, providing further electronic excitation transfer to luminescence centers, as evidenced by photoluminescence and scintillation measurements [6]. The effect of the Ga/Al ratio on the luminescence decay rate and other scintillation properties has been studied in single crystals of Gd$_1$Y$_2$Al$_{5-x}$Ga$_x$O$_{12}$:Ce, Gd$_2$Y$_1$Al$_{5-x}$Ga$_x$O$_{12}$:Ce, and Mg–co-doped Gd$_{3-y}$Y$_y$Al$_{5-x}$Ga$_x$O$_{12}$:Ce (GYAGG) grown by the micro-pulling down technique and in a ceramics form [7–13]. Disorder in the distribution of Al and Ga ions in oxygen-coordinated tetrahedra and octahedra ensures a possibility for engineering the bandgap and the crystal field strength acting on the activator ion and creating a diversity of sites for Ce activator localization in the matrix host [14]. The GYAGG

has a low density when the Gd/Y ratio provides the best performance. It results in a small photo-absorption coefficient of annihilation γ-quanta that are detected in widely used medical imaging positron emission tomography (PET) scanners. As a result, the material was discovered to be less competitive than LSO and LYSO scintillation crystals, which have been widely used in the latest generation of PET scanners that utilize the time-of-flight technique for detection [15].

Introducing lutetium (Lu) ions and creating the quaternary garnet composition would resolve this problem. Surprisingly, LY was measured for the composition $Lu_1Gd_2Al_2Ga_3O_{12}$:Ce (GLAGG) (30,600 ph/MeV), whereas scintillation kinetics had two components—75.7 ns (38%) and 326 ns (62%); a nearby LY value in $Lu_1Gd_2Al_2Ga_3O_{12}$:Ce (25,800 ph/MeV) was demonstrated further on [16]. A single crystal of the $Lu_2Gd_1Al_2Ga_3O_{12}$:Ce composition was grown by the Czochralski method and demonstrated an LY of 25,000 ph/MeV and scintillation decay constant of 53.6 ns [17]. The GLAGG:Ce scintillation films with a Lu/Gd ratio 1/1 demonstrated an LY at 145% of $Y_3Al_5O_{12}$:Ce; the material was found to be quite useful for alpha/gamma discrimination; however, the scintillation kinetics was slow [18]. Photoluminescence and scintillation kinetics were shown to be very different when transferring from Ce-doped LuAG to LuAGG [19]. At a concentration of Ce 0.2 at.%, LuAGG scintillation kinetics was evaluated by three components—15, 44, and 632 ns, correspondingly. In [20], quaternary garnets $YGd_2Al_2Ga_3O_{12}$:Ce and $LuGd_2Al_2Ga_3O_{12}$:Ce were compared. The light yield was measured to be 37,900 and 35,400 ph/MeV, correspondingly. However, slow components in the scintillation were observed through a strong dependence of the LY on a shaping time. A comparative study of $LuGd_2Al_2Ga_3O_{12}$:Ce and $Lu_2GdAl_2Ga_3O_{12}$:Ce single crystals was performed [21]. The $LuGd_2Al_2Ga_3O_{12}$:Ce sample demonstrated a LY of 35,400 ph/MeV, but its scintillation kinetics was found to be rather slow at 78 ns (42%) and 392 ns (58%), and, as a consequence, the time resolution was worse at 800 ps. Recently, authors [22,23] noticed a high light yield of the $(Gd,Lu)_3Al_2Ga_3O_{12}$:Ce (GLAGG) ceramic scintillator. Scintillation decay was shown to consist of three components: 75 ns, 190 ns, and 1300 ns. Despite the ability of Mg^{2+} co-doping to shape the photoluminescence and scintillation kinetics in GLAGG epitaxial films [24], the material was found to be slower than $(Gd,Y)_3Al_2Ga_3O_{12}$:Ce or LYSO, limiting its application in novel PET scanners.

Nevertheless, the quaternary GLAGG garnet would possess technological benefits. The melting temperature of the material is ~200 °C lower than that required for the LYSO, making the operational lifetime of the crucibles made from the precious metals longer. Moreover, GLAGG has a cubic spatial symmetry, which allows one to obtain a quality crystalline mass by different technological methods [25].

In-depth comprehensive studies have been performed over the past five years to improve the scintillation performance of GLAGG [26–30]. So far, it has not been possible to elucidate a generalized approach to stabilize the set of material parameters at a level exceeding the LYSO performance.

As a matter of fact, the incorporation of Lu in the garnet matrix creates some technological problems. First, one should note antisite centers due to a possible localization of small Lu^{3+} ions in the oxygen octahedra [31]. Further, the evaporation of the gallium during the compound synthesis can be diminished by the procedure of the raw material preparation [32].

In the current work, we focused on the study of the influence of the partial substitution of Gd with Lu ions in the Ce-doped GLAGG crystalline ceramics. The role of the creation of nonequilibrium carriers near various cationic subsystems in the quaternary compound was revealed, which made it possible to interpret scintillation kinetics and define technological actions for further improvement of the properties of this promising material. The study was supported by Monte-Carlo simulations of the energy transfer process, investigations of photo- and X-ray-excited luminescence spectra at different temperatures, measurements of light yield and photoluminescence and scintillation kinetics, and evaluation of afterglow effects.

2. Materials and Methods

2.1. Chemicals and Synthesis

Two sets of the fine powder garnet structure samples, either solely with Gd or with a partial substitution by Lu, were prepared by the coprecipitation method. The method consists of mixing all the desired components in a solution and the formation of a joint precipitate and, therefore, provides a homogeneous product, allowing phase formation at a lower temperature, which is favorable to diminish Ga evaporation. Solutions containing Gd, Lu, Ce, Al, and Ga nitrates were mixed in appropriate ratios to produce the desired compositions. The mixed solution was slowly added to a 2 mol/L solution of NH_4HCO_3 under constant stirring to form a precipitate. The precipitate was filtered, washed with water twice and with isopropyl alcohol once, dried at 100 °C in an air-ventilated oven for 8 h, and calcined at 850 °C for 2 h. Afterward, the powders were milled down to a median particle size of 1.0–1.5 μm in a planetary ball mill with corundum grinding media.

The composition of the samples investigated and their abbreviations are listed in Table 1. As well as the determination of the general set of the scintillation properties, to clarify the scintillation mechanism, the GAGG series of the samples targeted a study of the concentration dependence of the light yield (LY), photoluminescence, and scintillation kinetics. These results were used to define the optimal concentration of the activator for the GLAGG series. The GLAGG set was also prepared to ensure understanding of the technological factors that lead to phosphorescence.

Table 1. Composition of the samples under investigation.

GAGG Series	GLAGG Series
$Gd_{3-x}Al_2Ga_3O_{12}:Ce_x$ (x = 0.005 or 0.167 at.%) (G1)	$Gd_{1.195}Lu_{1.79+x}Al_2Ga_3O_{12}:Ce$ (x = 0.015 or 0.5 at.%) (GL1)
$Gd_{3-x}Al_2Ga_3O_{12}:Ce_x$ (x = 0.01 or 0.33 at.%) (G2)	$Gd_{1.493}Lu_{1.492+x}Al_2Ga_3O_{12}:Ce$ (x = 0.015 or 0.5 at.%) (GL2)
$Gd_{3-x}Al_2Ga_3O_{12}:Ce_x$ (x = 0.015 or 0.5 at.%) (G3)	$Gd_{1.2}Lu_{1.77+x}Al_2Ga_3O_{12}:Ce$ (x = 0.03 or 1 at.%) (GL3)
$Gd_{3-x}Al_2Ga_3O_{12}:Ce_x$ (x = 0.02 or 0.67 at.%) (G4)	$Gd_{1.2}Lu_{1.77+x}Al_2Ga_3O_{12}:Ce$ (x = 0.03 or 1 at.%) + 20 ppm (Mg), (GL4)
$Gd_{3-x}Al_2Ga_3O_{12}:Ce_x$ (x = 0.03 or 1 at.%) (G5)	$Gd_{1.26}Lu_{1.77+x}Al_2Ga_3O_{12}:Ce$ (x = 0.03 or 1 at.%)(GL5); the super-stochiometric additive of Gd
$Gd_{3-x}Al_2Ga_3O_{12}:Ce_x$ (x = 0.04 or 1.33 at.%) (G6)	$Gd_{1.26}Lu_{1.77+x}Al_2Ga_3O_{12}:Ce$ (x = 0.03 or 1 at.%) + 20 ppm (Mg) (GL6); the super-stochiometric additive of Gd
$Gd_{3-x}Al_2Ga_3O_{12}:Ce_x$ (x = 0.06 or 2 at.%) (G7)	$Gd_{1.2}Lu_{1.755+x}Al_2Ga_3O_{12}:Ce$ (x = 0.045 or 1.5 at.%) (GL7)
	$Gd_{1.26}Lu_{1.755+x}Al_2Ga_3O_{12}:Ce$ (x = 0.045 or 1.5 at.%) (GL8); the super-stochiometric additive of Gd

Contrary to single crystals, for which the concentration of the activator in the crystal is typically less than x = 0.002, in this series, we focused on the high concentration of Ce achievable exclusively in the ceramics. The results of [33] demonstrated that segregation of Ce ions along the boundaries of the grains occurs. However, a fraction of such Ce ions is too small to affect the scintillation parameters. The change in properties with Ce concentration was evaluated using a simpler GAGG ternary crystalline system, and then a less variable concentration range was used in the preparation of GLAGG samples.

Ceramic samples were prepared from the powders to evaluate the scintillation parameters of the materials. A size of 1.5 mm-thick green bodies of 20 mm in diameter were prepared by uniaxial pressing at 64 MPa. The tablets were sintered in air for 2 h at 1600 °C. The resulting ceramic samples were translucent and had ~97–98% of the theoretical density. The samples were ground to a thickness of 1 mm for the study of their scintillation properties. Polishing of the samples was carried out on a POLYLAB P12M machine. For finishing polishing, Kemet Aquapol-M diamond suspensions were used. Thermal etching of the samples was carried out at a temperature of 1250 °C for 10 min in a Linn EVA 1700 oven.

2.2. Instrumentation

Samples were evaluated for luminescent and scintillation properties. The photoluminescence (PL) kinetics were measured with the PicoQuant Fluotime 250 spectrofluorometer under pulsed LED excitation with a pulse width (FWHM) shorter than 600 ps at 340 and 450 nm and the luminescence detection at 550 nm with a spectral width of 10 nm. Room temperature scintillation kinetics were measured with a ^{22}Na source by the start-stop method with XP2020 photomultipliers in both channels, providing a response function width (FWHM) of 1.2 ns. The first three channels, corresponding to the triple response function width, were excluded from consideration at the approximation of the scintillation kinetics. The change in the light yield (LY) in the GAGG and GLAGG series was evaluated by the measurement of the full absorption peak position of ^{241}Am alpha-particles as used for the measurements with translucent or powdered samples in [34]. A $Y_3Al_5O_{12}$:Ce (YAG) single crystal of 1 mm thick with grinded surfaces and a LY of 20,600 ph/MeV was chosen as a reference sample. The errors in light yield measurements were defined to be $\pm2\%$, whereas fitting results for decay constants fit ±2 ns, correspondingly. In addition, the radio-luminescence (RL) properties of several fabricated samples were evaluated under excitation by X-rays of apparatus URS-55A equipped with an X-ray tube BSV-2 (Cu anode, 30 kV, 10 mA). The luminescence was dispersed using the LOMO monochromator MDR-23 (spectral width of 2 nm) and detected by the photomultiplier FEU-106 in a photon-counting mode. Spectra were corrected for the spectral sensitivity of the registration bench. The bench has been used for RL temperature dependence and thermo-stimulated luminescence (TSL) measurements above room temperature.

3. Results and Discussion

3.1. Microstructure Properties

A comparison of SEM images of a typical ceramics sample (G3, GL2) obtained with Jeol JSM 7100 F at 20 kV accelerating voltage is presented in Figure 1. The sample demonstrates grains of garnet habitus, confirming the phase homogeneity of the ceramics. Different contrasts on the backscattered electron image (Figure 1b,d) correspond to different grain orientations. As seen, both types of ceramics have a practically similar microstructure of chaotically oriented grains.
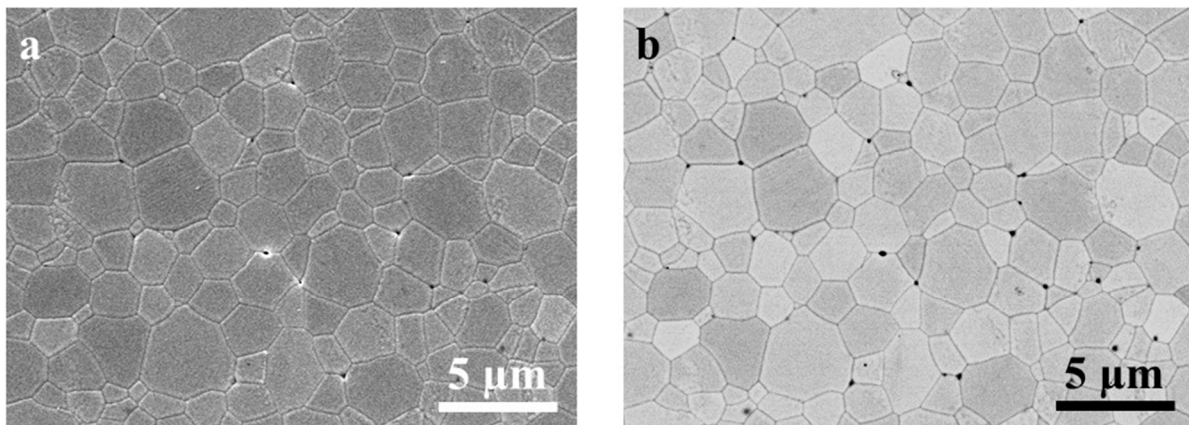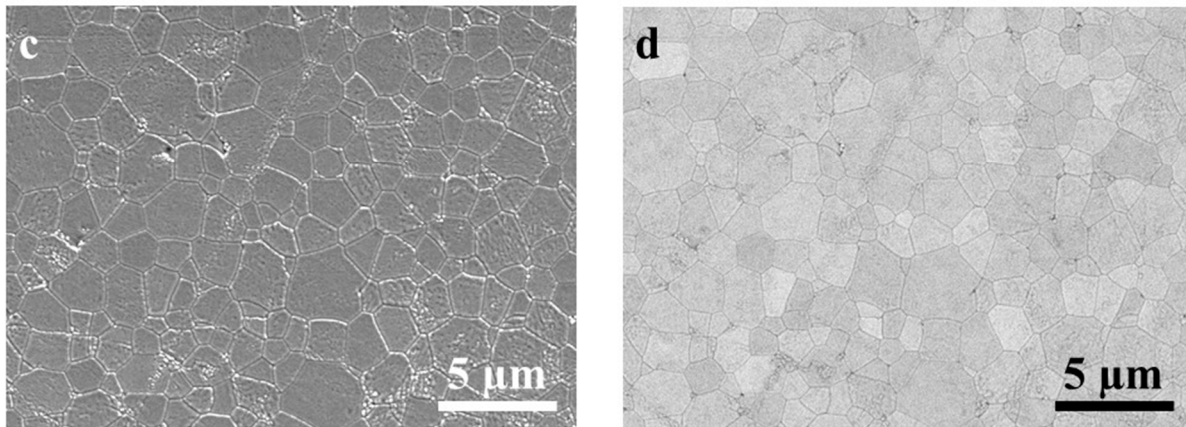

Figure 1. *Cont.*

Figure 1. SEM images of $Gd_{1.5}Lu_{1.5}Al_2Ga_3O_{12}$:Ce (GL2) (**a,b**) and $Gd_3Al_2Ga_3O_{12}$:Ce (G3) (**c,d**) ceramics in secondary electron and backscattered electron modes, respectively. Images obtained in backscattered electron mode (**b,d**) demonstrate random orientation of crystallites in the ceramics.

3.2. Results on GAGG:Ce Series

Figure 2 shows photo-luminescence kinetics of GAGG series measured at excitation to the Ce^{3+} $5d_2$ state (3.67 eV) at room temperature.
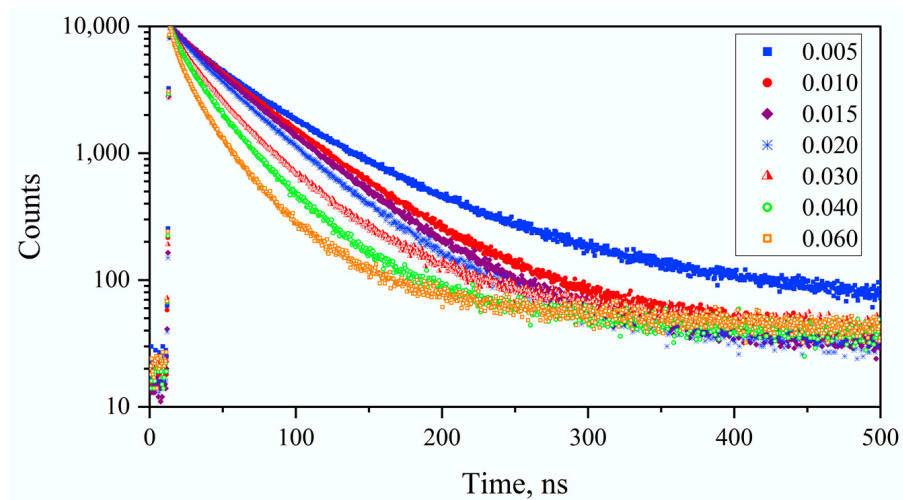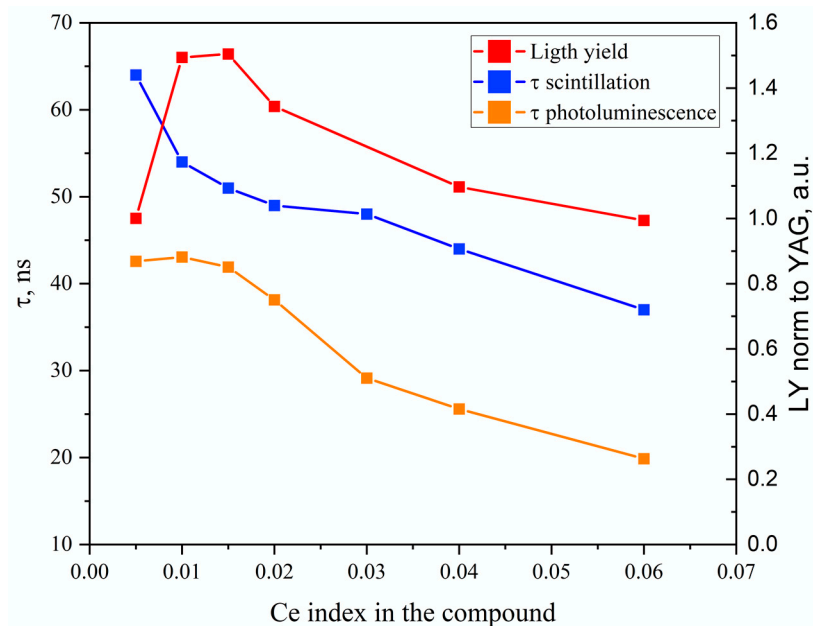

Figure 2. Photoluminescence kinetics of GAGG series at 3.67 eV excitation measured at room temperature. Ce index of G1–G7 samples is indicated.

At excitation to the $5d_2$ level, which overlaps the bottom of the conduction band in Al/Ga mixed garnet structure materials [35], the cerium center is partially autoionized and an electron can be captured by shallow traps. Thus, at the lowest Ce concentration, photo-luminescence kinetics has a remarkable tail. In the range of the Ce index, x = 0.01–0.02, and the initial part of the kinetics remains close to a single exponential, whereas a further Ce index increase in the composition makes decay shorter, indicating a concentration quenching. Figure 3 shows the scintillation kinetics of representative samples of the GAGG series measured at room temperature. A low concentration sample shows remarkable phosphorescence. Its presence might be characterized by a larger number of coincidences due to increasing the rate of the pulses detected prior to the scintillation [36].
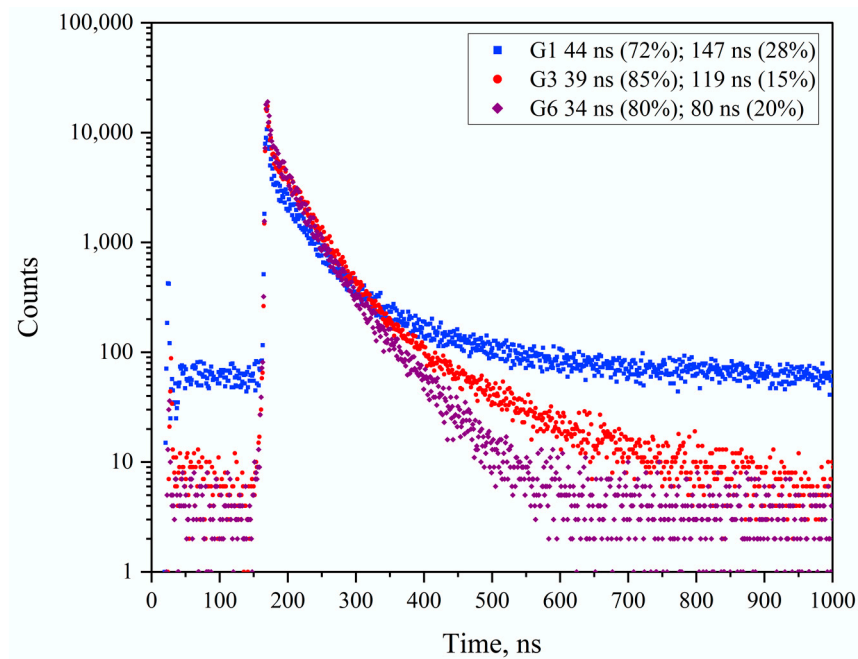
Figure 3. Scintillation kinetics of G1, 3, 6 samples of GAGG series measured at room temperature.

A shortening of the luminescence kinetics due to concentration quenching is accompanied by a luminescence quantum yield decrease, which affects the yield of scintillations as well. Figure 4 summarizes the results of the GAGG series. In our consideration, we compared the effective decay constant (<τ> photoluminescence) calculated for the initial part of the photoluminescence kinetics in the time interval 200 ns with the effective scintillation decay time (<τ> scintillation), which is defined to be $<\tau> = \sum_i \tau_i f_i$. The parameter f_i is a fraction of the component τ_i. Parameter <τ> scintillation is of particular interest; it has a practical importance to define an integration time at the detection. The LY measured with samples having different Ce indexes is shown as well.

Figure 4. Concentration dependence of the scintillation light yield and an effective decay time of the initial part of the photoluminescence and the scintillation kinetics in GAGG series measured at room temperature.

3.3. Results on GLAGG:Ce Series

Figure 5 summarizes the results on luminescence and scintillation kinetics measurements of the GLAGG series. A detailed analysis of photoluminescence kinetics was performed by approximation with a larger number of exponential functions. The results are shown in convenient coordinates: x—decay constant, y—its fraction to see the trend in a change. In general, it is characterized by three decay components: the fast one, having a decay constant of ~10 ns; a dominating component, with a decay constant of ~40 ns; and a slow component, with a decay of ~160 ns. The distribution of the decay constants in Figure 5a shows that super-stochiometric additives (GL5,8), introducing a small amount of aliovalent cooping (GL4) or their combined application (GL6) in the composition, have a weak influence on photoluminescence kinetics.


(**a**)

(**b**)

(**c**)

(**d**)

(**e**)
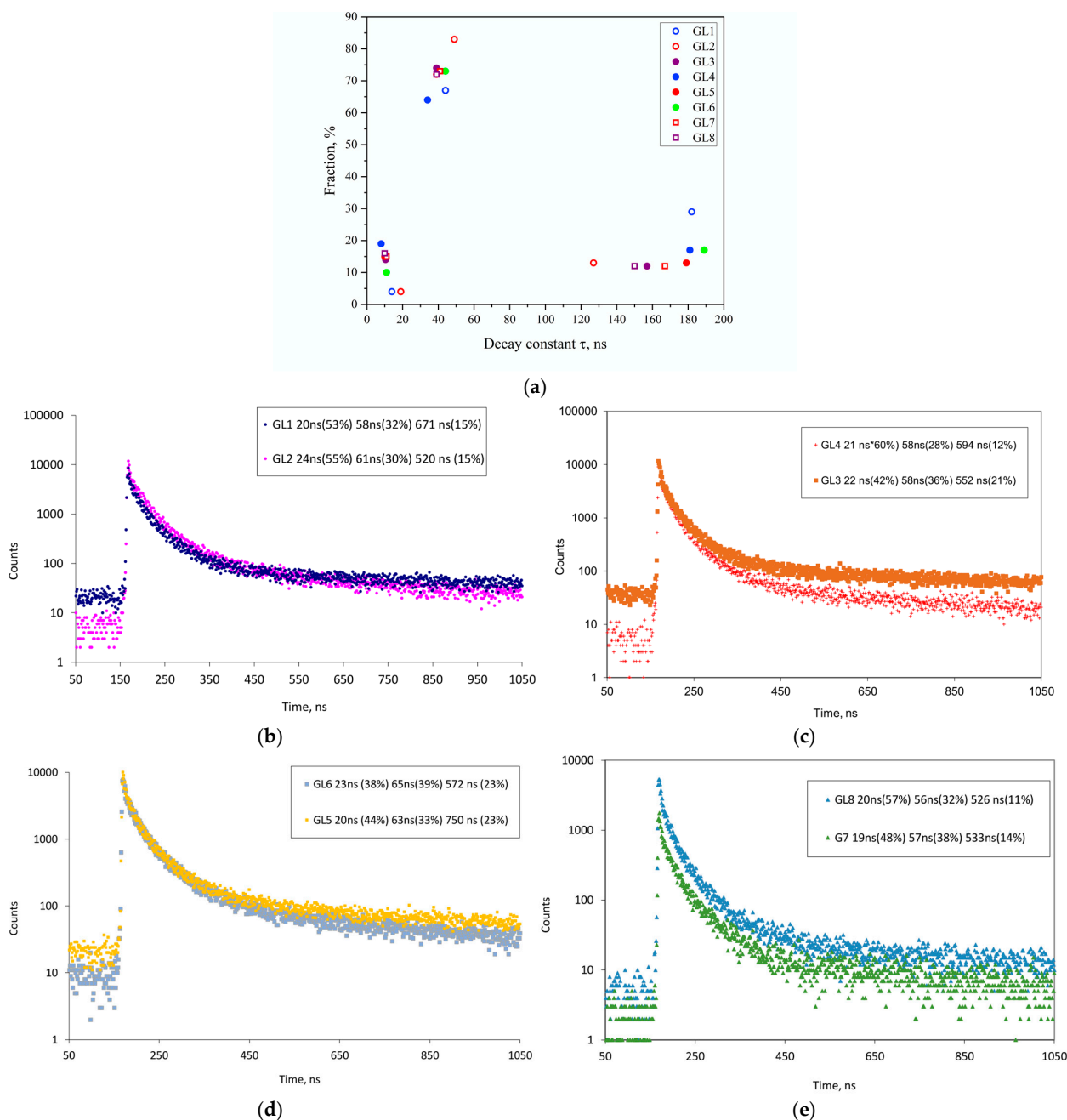
Figure 5. Distribution of the decay constants and their fractions in the photoluminescence kinetics at 340 nm excitation in GLAGG samples (**a**) and scintillation kinetics of samples (**b**–**e**) measured at room temperature.

Based on the results of the GAGG series, the range of the Ce index in the GLAGG series was chosen to be in the range compromising between LY drop and faster scintillation kinetics. In scintillation, a fast component of ~20 ns becomes dominating, whereas a slower component of ~60 ns shows a decrease in its contribution to the level of ~30%. Nonetheless, scintillation of GLAGG at relatively high Ce concentrations is characterized by the presence of fast and slow stages of the scintillation kinetics with decay constants that differ by an order of magnitude.

Furthermore, the decay components and their fractions are barely dependent on the concentration of Ce in the range of x = 0.015 to 0.045; the co-dopant presence in the composition or the presence a super-stochiometric additive. As seen from the comparison of the number of coincidences detected prior to the scintillation pulse in Figure 5, the small concentration additive of Mg, similarly to the case of single crystals of the GAGG family, suppresses phosphorescence. The same effect is observed at the super-stochiometric additive of Gd in the composition.

The sample GL1, which displays bright phosphorescence after exposure to an X-ray source, was evaluated for a TSL above room temperature. Figure 6a depicts typical luminescence and luminescence excitation spectra in GLAGG. The phosphorescence spectrum coincides with Ce^{3+} luminescence and the TSL spectrum shows a strong thermo-activation band peaked near 340 K (Figure 6b,c).

(a)

(b)

(c)
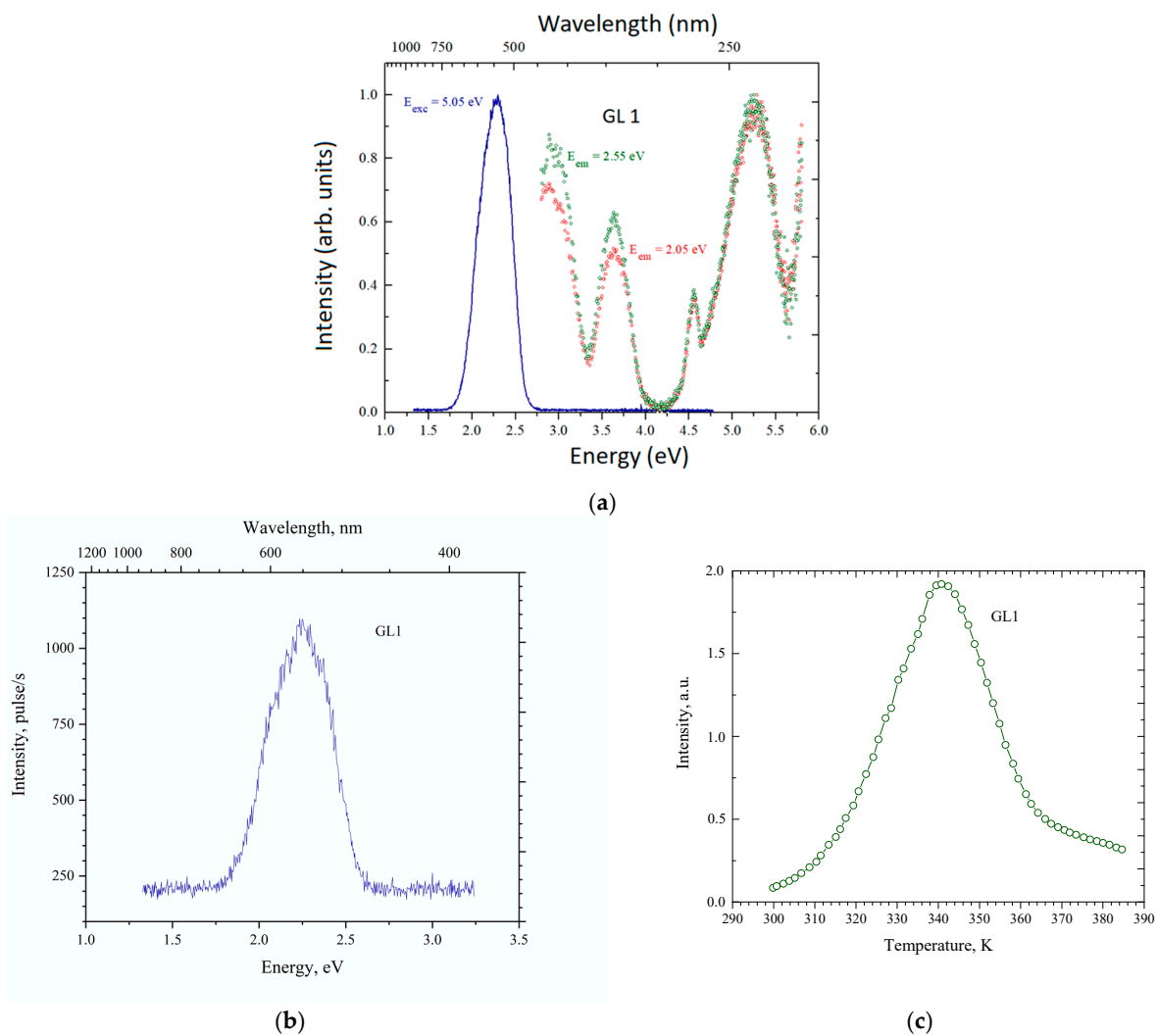
Figure 6. Luminescence and luminescence excitation spectra measured at RT—(**a**), phosphorescence spectrum after the termination of the X-ray excitation—(**b**), TSL curve measured above RT at 540 nm—(**c**).

It should be noted that the position of the TSL band correlates rather well with the maximum in the RL yield temperature dependence. As an example, Figure 7 demonstrates the temperature dependence of the RL yield measured with GL1 and GL2 samples. The higher the Lu content in the ceramics, the more pronounced the peak is.
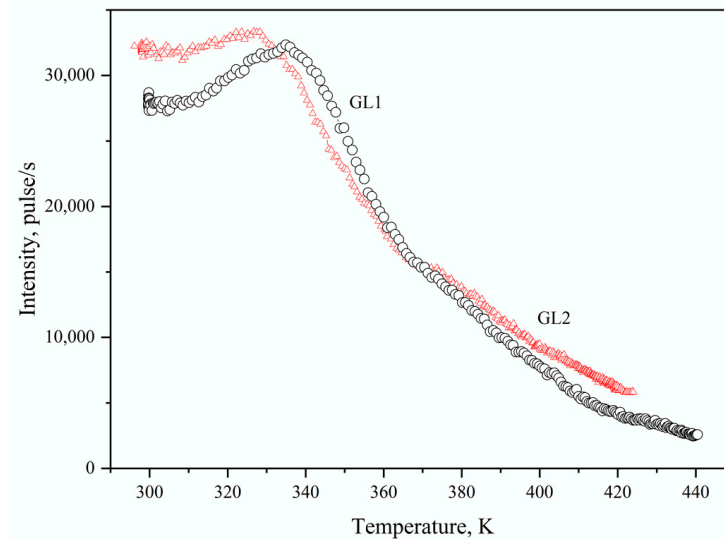

Figure 7. Temperature dependence of RL yield measured at registration at 2.3 eV (540 nm) with GL1 and GL2 samples.

3.4. Monte-Carlo Simulation of Excitation Transfer in GAGG:Ce and GLAGG:Ce

Results shown in Figure 5 demonstrate evidence that phosphorescence, whose presence is characterized by a background created by coincidences detected prior to the scintillation, is not an intrinsic property of quaternary Ce-doped Gd-Lu garnets. The technological actions, including co-doping with a small quantity of aliovalent Mg^{2+} ions or super-stochiometric additives of Gd, diminish the role of the defects created either under evaporation of Ga at high-temperature treatment or antisite defects in the electronic excitation's relaxation.

A distinctive feature of GLAGG in comparison with GAGG is the presence of a third long phase in the scintillation decay kinetics, which also does not manifest itself in photoluminescence. An essential difference between GLAGG in comparison with GAGG is the gadolinium sublattice under conditions of broken integrity. At the conditions of integrity, an interaction associated with the excitations of the $5d^04f^7$ configuration of the Gd^{3+} ions and Ce^{3+} activator is described by the dipole-dipole interaction energy transfer. At the same time, diffusion over the states of gadolinium also occurs due to the dipole-dipole transfer between f-states. Thus, the energy transfer can be a diffusion-controlled dipole-dipole transfer. However, the well-known solutions to the transfer problem based on interpolation formulas [37,38] are of limited use in the case under consideration since the migration of excitations along the gadolinium sublattice has a hopping character. The event of Gd^{3+} interaction directly with the activator, in addition to the dipole-dipole transfer, should also consider the exchange (Dexter) interaction.

A Monte-Carlo migration calculation model, accounting for the real crystallographic structure of garnet, in which the distances between gadolinium ions form well-defined cationic coordination spheres [39] (Figure 8), was used. Obviously, at a low concentration of gadolinium, the connectivity of the lattice positions along which hopping migration occurs is disrupted.
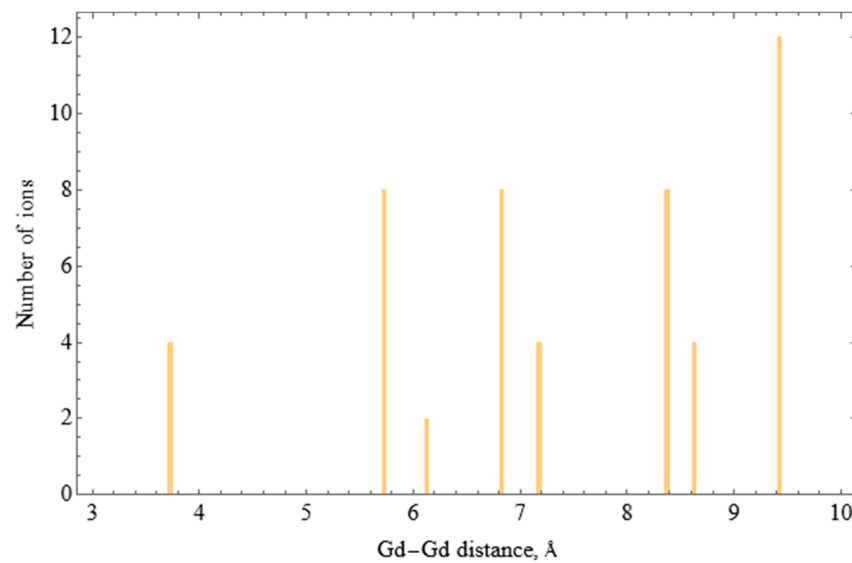
Figure 8. Number of gadolinium ions in various Gd-Gd cationic coordination spheres in the GAGG structure.

The expressions for probabilities of excitation hops between gadolinium ions $w_{Gd \rightarrow Gd}$ and from the Gd^{3+} ion to the Ce^{3+} $w_{Gd \rightarrow Ce}$ ion and the ranges of the parameters were chosen in accordance with [40–44]:

$$
\begin{aligned}
w_{Gd \rightarrow Gd}(r) &= \frac{1}{\tau_{Gd}} \frac{R^6_{d-d,Gd \rightarrow Gd}}{r^6} + c_{Gd \rightarrow Gd} \exp\left(-2 \frac{r}{\alpha_{Gd \rightarrow Gd}}\right), \\
w_{Gd \rightarrow Ce}(r) &= \frac{1}{\tau_{Gd}} \frac{R^6_{d-d,Gd \rightarrow Ce}}{r^6} + c_{Gd \rightarrow Ce} \exp\left(-2 \frac{r}{\alpha_{Gd \rightarrow Ce}}\right).
\end{aligned}
\tag{1}
$$

where $\tau_{Gd} = 4 \times 10^{-4}$ s, $R_{d-d,Gd \rightarrow Gd} = 1$ nm, $R_{d-d,Gd \rightarrow Ce} = 1.4$ nm, $c_{Gd \rightarrow Gd} = 1.9 \times 10^{15}$ s^{-1}, $c_{Gd \rightarrow Ce} = 2.1 \times 10^{13}$ s^{-1}, $\alpha_{Gd \rightarrow Gd} = 0.04$ nm, $\alpha_{Gd \rightarrow Ce} = 0.063$ nm. Photoluminescence kinetics parameters obtained from the data in Figures 3 and 6a were used as well.

A supercell consisting of $3 \times 3 \times 3$ garnet unit cells containing 648 gadolinium positions for two gadolinium indexes y in $(Gd_y Lu_{1-y})_3 Al_2 Ga_3 O_{12}$ (GLAGG): $y = 1$ and 0.4 was used in the simulation. The location of gadolinium ions at a concentration of less than 100% was chosen randomly. In accordance with the chosen cerium index ($x = 0.015$, 0.03, or 0.045), which corresponds to cerium concentrations of 0.5, 1.0, and 1.5 at.%, an appropriate number of gadolinium ions (3, 6, or 10) were randomly replaced by cerium. For the simulation, one of the randomly selected gadolinium ions in the supercell was set excited; afterward, excitation hopping was simulated with a probability determined by the distances to all ions, considering the exchange interaction. The time when excitation reaches the Ce^{3+} ion was calculated for 10^5 realizations.

Figure 9 shows the intensity of the arrival of excitation on cerium in GAGG and GLAGG for a few Ce^{3+} concentrations. The energy transfer to cerium proceeds in a substantially nonexponential manner in time; in all cases, there is a fast component associated with the transfer to cerium from a nearby excited gadolinium ion. At a high concentration of gadolinium in the composition, the longer tail part arises due to diffusion through the regular gadolinium subsystem. However, as the Gd concentration decreases, the connectivity of the network along which diffusion occurs decreases, and the rate of excitation arrival at cerium becomes nonexponential and has a slower tail part.
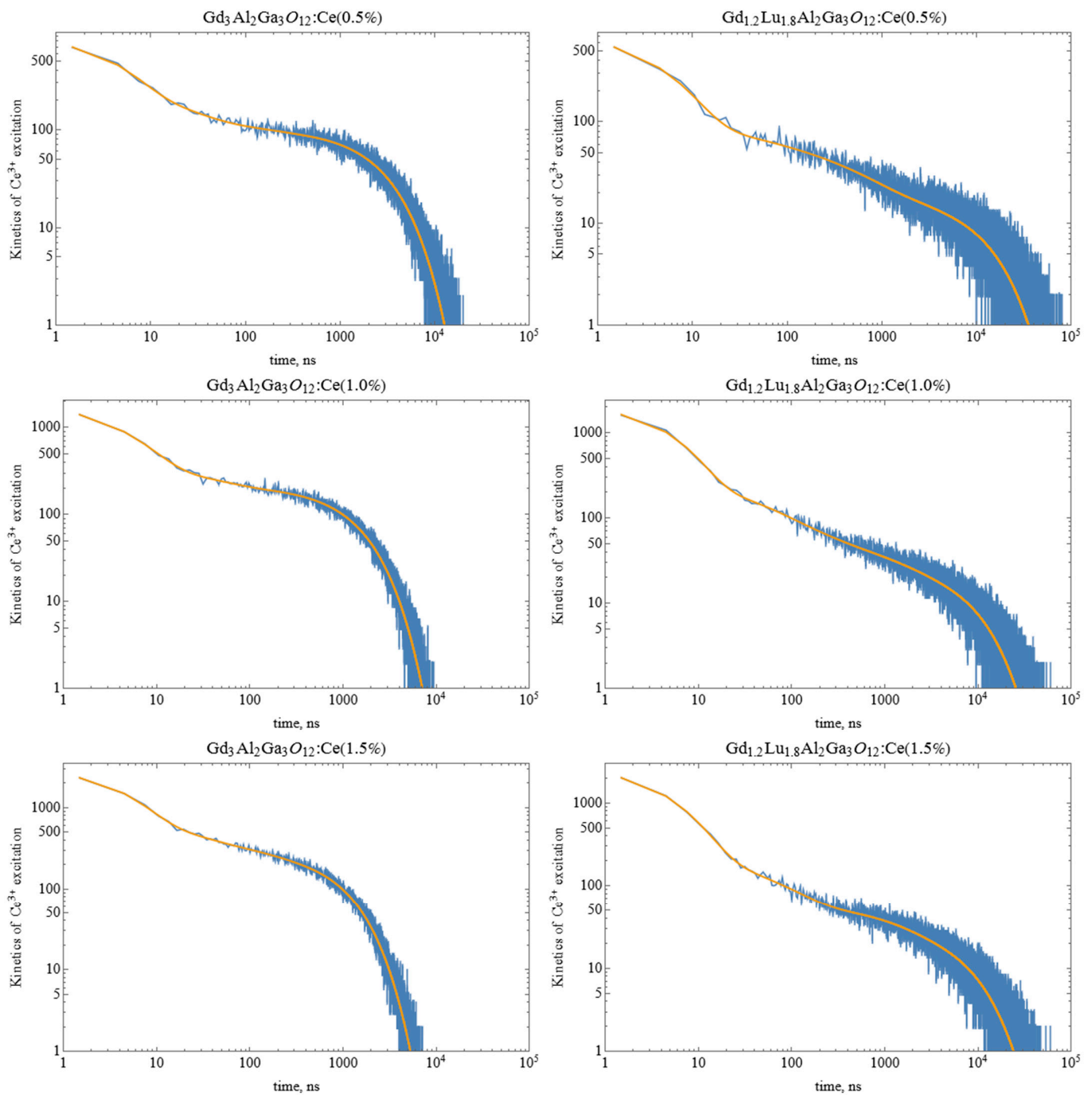
Figure 9. Time dependence of the populating intensity of the excited $5d_1$ states of Ce^{3+} in the case when excitation appears at the f-subsystem of the gadolinium ion at the time $t = 0$ in GAGG (panels on the left) and GLAGG (panels on the right) on Ce concentration (indicated). Yellow curves—approximation by the sum of the exponential functions, which were obtained by expansion into a set of exponents with different characteristic times from 1 ns to 10^5 ns as described in Equation (2). Bin width at simulation was chosen to be 0.5 ns.

The intensity of the excitation arrival on cerium was decomposed by many exponential functions, the characteristic times of which are uniformly distributed over the logarithm from 1 ns to 100 µs as expressed:

$$I_{Gd \to Ce}(t) = \sum_n \frac{A_n}{\tau_n} \exp\left(-\frac{t}{\tau_n}\right). \tag{2}$$

In this case, the analysis was carried out using regularization according to Tikhonov [45].

The desired luminescence kinetics of Ce^{3+} ions were obtained by convolving expression (2) with the decay law of Ce^{3+} luminescence measured and characterized by a set of single exponential functions with decay constants τ_{Ce}:

$$I_{Ce}(t) = \sum_n \frac{A_n}{\tau_{Ce} - \tau_n} \left(\exp\left(-\frac{t}{\tau_{Ce}}\right) - \exp\left(-\frac{t}{\tau_n}\right) \right). \tag{3}$$

The incorporation of Lu ions into the lattice leads to an increase in the role of scintillation mechanisms, which are realized due to interaction with self-trapped states of the lattice: excitons (STE) and holes (STH). STE sensitizes the luminescence of Ce^{3+} ions [25]:

$$STE + Ce^{3+} \rightarrow Ce^{3+*} \rightarrow Ce^{3+} + h\nu. \tag{4}$$
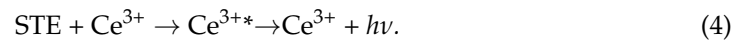
In the Lu-rich GLAGG compounds considered in this work, the Gd sublattice is broken and less efficient for converting STE into mobile Frenkel-type excitons (see, e.g., [46]). In fact, Gd^{3+} individually competes with Ce^{3+} ions for exciton trapping. However, the oscillator strength of the inter-configuration *d–f* transition of Ce^{3+} is about one hundred times higher than that of the *f–f* transitions of Gd^{3+} ions, which makes their chances of capture almost equal, despite the large difference in concentrations. Figure 10 demonstrates results of the simulation of the contribution of different transfer mechanisms to Ce^{3+} ions from the Gd sublattice and STE and the resulted luminescence kinetics at a few concentrations of Ce^{3+} ions in the compound. The rate of STE to Ce^{3+} transfer for a concentration of 1% of cerium was chosen to be 10 times larger than the rate of conversion of STE to *f–f* excitation of gadolinium.
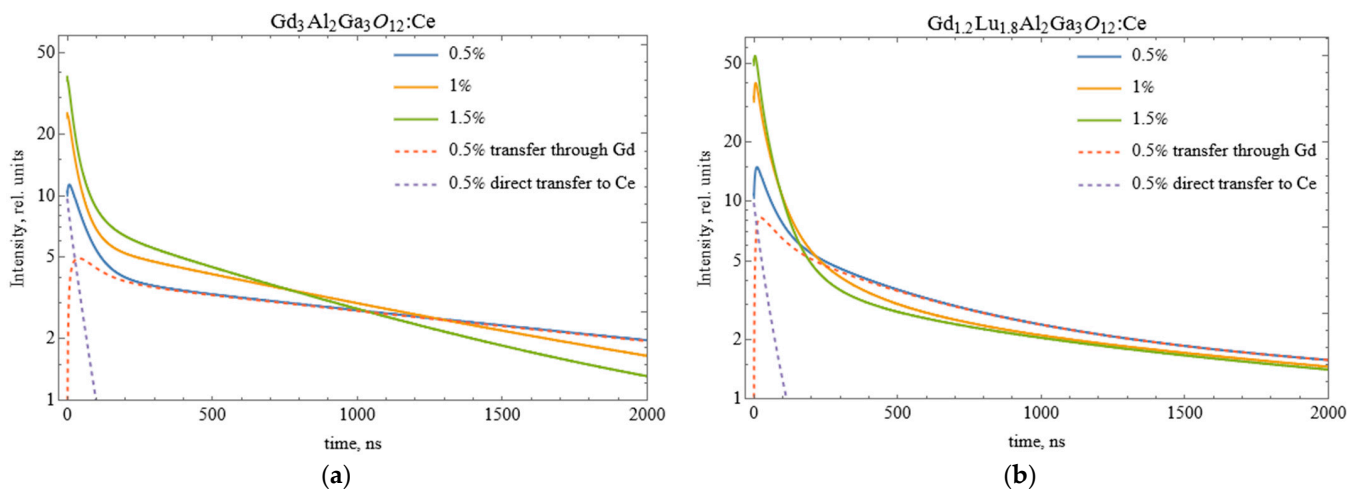
Figure 10. Results on the simulation of the scintillation kinetics of GAGG (**a**) and GLAGG (**b**) on Ce concentration (indicated). Dashed curves show a contribution of the mechanisms of the electronic excitations transfer via the Gd sublattice and a direct transfer from STE at Ce concentration of 0.5 at.%. The integrals under the kinetics are the same.

In GAGG, the scintillation kinetics has two distinguished phases called τ_{fast} and $\tau_{medium\text{-}fast}$. Their decay constants decrease with an increase in the Ce concentration in the compound, which is in good agreement with the experimental data (Figures 3 and 11).
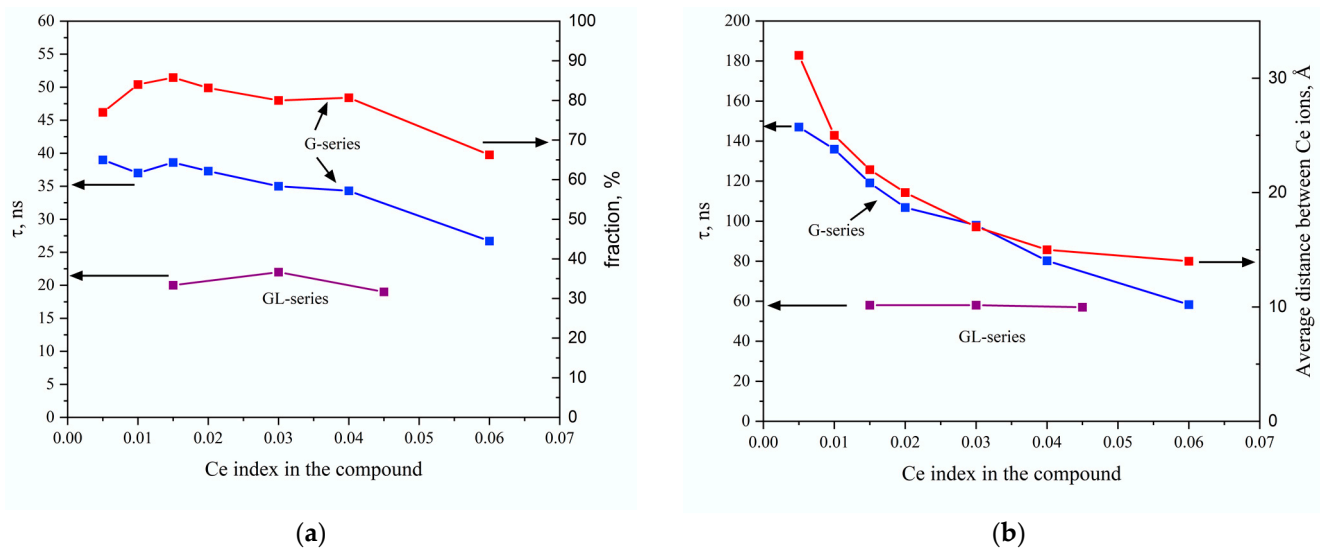
Figure 11. Concentration dependence of fast (**a**) and medium-fast (**b**) scintillation decay constants in GAGG samples (G-series) in a comparison with GLAGG samples (G1,3,7). An average distance between Ce ions in GAGG calculated in a homogeneous distribution approximation is shown in panel (**b**).

When the gadolinium sublattice is diluted in GLAGG, the fractions of both phases in the scintillation kinetics are less dependent on the Ce concentration, which correlates well with experimental data presented in Figure 11a,b.

A change in the decay time of the $\tau_{\text{medium-fast}}$ component in the kinetics of scintillations in GAGG correlates well with a decrease in the average distance between Ce ions in GAGG (Figure 11b). Apparently, it occurs with an increase in the Ce index in the compound because the region of the gadolinium subsystem in which hopping migration occurs is significantly reduced; the prompt capture of excitations by cerium ions begins to dominate.

*3.5. The Origin of the Slow Component of GLAGG:Ce*

As seen, the fast and medium-fast scintillation components in GLAGG are weakly dependent on Ce concentration, which correlates well with the experimental results. However, the diminished role of the Gd subsystem in the delivery of electronic excitations to Ce^{3+} ions causes a drop in LY. Table 2 summarizes light yield measured with samples of the GL series. Systematically, a super-stoichiometric additive and co-doping decrease the light yield, which is in line with the results of [47,48]. Worth noting, when Gd is completely removed from the crystal matrix, the ternary Lu-Al-Ga garnet demonstrates a LY at the level of YAG or even worse [1].

Table 2. Relative light yield of GLAGG samples.

Sample	GL1	GL2	GL3	GL4	GL5	GL6	GL7	GL8
LY relative to YAG:Ce with grinded surfaces (20,600 ph/MeV)	1.45	1.31	1.18	1.13	1.11	1	1.13	1

When lutetium ions are introduced into the lattice, the ionization density is reshuffled significantly. Lutetium has a high nuclear charge (Z = 71), greater than that of Gd (Z = 64). Therefore, the probability of formation of photoelectrons due to primary interactions with gamma-quanta in the compound near Gd and Lu ions is expected to be 1:1.5 due to $\sim Z^4$ cross-section dependence. Heavy ions, as per Bragg's additivity rule, provide a larger contribution to ionization losses of the photoelectron. Thus, a sequential capture

mechanism for the excitation of Ce^{3+} ions, which is controlled by the hole mobility, should be assumed:

$$e^- + STH + Ce^{3+} \rightarrow Ce^{4+} + e^- \rightarrow Ce^{3+*} \rightarrow Ce^{3+} + h\nu, \qquad (5)$$
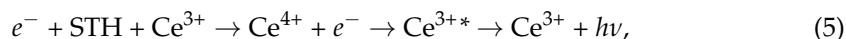
where Ce^{4+} is a dynamical state of the Ce ion.

The predominant self-localization of holes in polyhedra around lutetium ions in GLAGG with a highly diluted Gd sublattice limits their participation in migration along the gadolinium sublattice with an effective participation in transformation into Frenkel-type excitons. The capture of holes by Ce^{3+} ions having a ground state above the top of the valence band of ~3 eV [35] is of a low probability. Therefore, process (5) may be responsible for the slowest component in GLAGG scintillation. The slowest decay component in the scintillation (500–700 ns), as seen from data in Figure 6, is slightly affected by variation of the technological factors; therefore, its decreasing fraction is a matter of improving the mobility of the holes in the compound. In GYAGG, when the gadolinium sublattice is diluted by Y ions, the scintillation kinetics is well approximated by two fast and medium-fast components; no slow component is observed. Light yttrium ion (Z = 36) provides the probability of the formation of photoelectrons upon interaction with gamma-quanta in the compound ten times lower than that of Gd ions. Therefore, the ionization within the Gd sublattice still dominates in GYAGG.

The results obtained correlate with the observation of the slowing of the scintillation kinetics at the incorporation of the Lu ions into the matrix host in the simpler oxide compounds [49]. An increase in the fraction of lutetium in the perovskite $(Y,Lu)AlO_3$:Ce provides a scintillation component with a decay constant of 400 ns. It is worth noting that the partial substitution of yttrium with lutetium changes the scintillation yield as well. The best light yield [50] has been measured when 40% of Y was replaced by Lu in the composition.

Despite, thus, the prominent fast component in the scintillation, the severe dilution of the Gd^{3+} sublattice with Lu^{3+} in the compound leads to combining two effects, namely the decrease in the light yield and the appearance of the slow component in the scintillation. An increase in the Ce concentration in the ceramics does not promote a suppression of the slow component in the scintillation as well. The slow decay component in the scintillation varies in the range of 500–700 ns and having a fraction in the scintillation kinetics above 10% is a little dependent on the technological conditions: co-doping with Mg^{2+} and variation of the stoichiometry. Therefore, further development of the material should be targeted for the search of the compound composition to obtain a balance between mechanisms, providing the best combination of light yield and a minimal level of the slow part of the scintillation kinetics.

4. Conclusions

The scintillation properties of ceramic samples of $(Gd,Lu)_3Al_2Ga_3O_{12}$ and $Gd_3Al_2Ga_3O_{12}$ doped by Ce were evaluated. We focused on the effects responsible for different stages of radiative relaxation and having technological and physical origins. As was expected, technological actions like super-stoichiometric additives of gadolinium in the material composition or its co-doping with a low concentration of Mg provide suppression of the phosphorescence in the material, which is quite similar to observations made for ternary $Gd_3Al_2Ga_3O_{12}$:Ce and quaternary $(Gd,Y)_3Al_2Ga_3O_{12}$:Ce scintillators. It demonstrates that phosphorescence is not an intrinsic property of such materials.

An increase in the compositional disorder in the crystal upon partial substitution of gadolinium with lutetium ions triggers additional mechanisms for the transfer of excitations of nonequilibrium carriers to Ce^{3+} ions.

The Monte-Carlo simulation of electronic excitation transfer demonstrates that breaking the integrity of the gadolinium sublattice increases the role of self-trapped states in the excitation of Ce^{3+} ions. They enhance an increase in the fraction of short and very long components in the scintillation kinetics.

References

1. Kamada, K.; Endo, T.; Tsutumi, K.; Yanagida, T.; Fujimoto, Y.; Fukabori, A.; Yoshikawa, A.; Pejchal, J.; Nikl, M. Composition Engineering in Cerium-Doped $(Lu,Gd)_3(Ga,Al)_5O_{12}$ Single-Crystal Scintillators. *Cryst. Growth Des.* **2011**, *11*, 4484–4490. [CrossRef]
2. Kamada, K.; Yanagida, T.; Pejchal, J.; Nikl, M.; Endo, T.; Tsutumi, K.; Fujimoto, Y.; Fukabori, A.; Yoshikawa, A. Scintillator-oriented combinatorial search in Ce-doped $(Y,Gd)3(Ga,Al)5O12$ multicomponent garnet compounds. *J. Phys. D Appl. Phys.* **2011**, *44*, 505104. [CrossRef]
3. Kamada, K.; Yanagida, T.; Endo, T.; Tsutumi, K.; Usuki, Y.; Nikl, M.; Fujimoto, Y.; Fukabori, A.; Yoshikawa, A. 2 inch diameter single crystal growth and scintillation properties of $Ce:Gd_3Al_2Ga_3O_{12}$. *J. Cryst. Growth* **2012**, *352*, 88–90. [CrossRef]
4. Kamada, K.; Kurosawa, S.; Prusa, P.; Nikl, M.; Kochurikhin, V.V.; Endo, T.; Tsutumi, K.; Sato, H.; Yokota, Y.; Sugiyama, K.; et al. Cz grown 2-in. size $Ce:Gd3(Al,Ga)5O12$ single crystal; relationship between Al, Ga site occupancy and scintillation properties. *Opt. Mater.* **2014**, *36*, 1942–1945. [CrossRef]
5. Korzhik, M.; Alenkov, V.; Buzanov, O.; Dosovitskiy, G.; Fedorov, A.; Kozlov, D.; Mechinsky, V.; Nargelas, S.; Tamulaitis, G.; Vaitkevičius, A. Engineering of a new single-crystal multi-ionic fast and high-light-yield scintillation material $(Gd_{0.5}-Y_{0.5})_3Al_2Ga_3O_{12}:Ce,Mg$. *CrystEngComm* **2020**, *22*, 2502–2506. [CrossRef]
6. Korzhik, M.; Borisevich, A.; Fedorov, A.; Gordienko, E.; Karpyuk, P.; Dubov, V.; Sokolov, P.; Mikhlin, A.; Dosovitskiy, G.; Mechninsky, V.; et al. Uglov, The scintillation mechanisms in Ce and Tb doped $(Gd_xY_{1-x})Al_2Ga_3O_{12}$ quaternary garnet structure crystalline ceramics. *J. Lumin.* **2021**, *234*, 117933. [CrossRef]
7. Solodovnikov, D.; Weber, M.; Haven, D.; Lynn, K. Single crystal Ce doped scintillator material with garnet structure sensitive to gamma ray and neutron radiation. *J. Cryst. Growth* **2012**, *52*, 99–102. [CrossRef]
8. Chewpraditkul, W.; Pánek, D.; Brůža, P.; Chewpraditkul, W.; Wanarak, C.; Pattanaboonmee, N.; Babin, V.; Bartosiewicz, K.; Kamada, K.; Yoshikawa, A.; et al. Luminescence properties and scintillation response in Ce^{3+} doped $Y_2GdAl_{5-x}Ga_xO_{12}$ (x 5 2, 3, 4) single crystals. *J. Appl. Phys.* **2014**, *116*, 083505. [CrossRef]
9. Chewpraditkul, W.; Brůža, P.; Pánek, D.; Pattanaboonmee, N.; Wantong, K.; Chewpraditkul, W.; Babin, V.; Bartosiewicz, K.; Kamada, K.; Yoshikawa, A.; et al. Optical and scintillation properties of Ce^{3+}-doped $YGd2Al5xGaxO12(x\frac{1}{4}2,3,4)$ single crystal scintillators. *J. Lumin.* **2016**, *169*, 43–50. [CrossRef]
10. Chewpraditkul, W.; Pattanaboonmee, N.; Chewpraditkul, W.; Sakthong, O.; Yamaji, A.; Kamada, K.; Kurosawa, S.; Yoshikawa, A.; Drozdowski, W.; Witkowski, M.E.; et al. Scintillation Characteristics of Mg^{2+}-Codoped $Y_{0.8}Gd_{2.2}(Al_{5-x}Ga_x)O_{12}:Ce$ Single Crystals. *IEEE Trans. Nucl. Sci.* **2020**, *67*, 910–914. [CrossRef]
11. Cherepy, N.J.; Payne, S.A.; Asztalos, S.J.; Hull, G.; Kuntz, J.D.; Niedermayr, T.; Pimputkar, S.; Roberts, J.J.; Sanner, R.D.; Tillotson, T.M.; et al. Scintillators With Potential to Supersede Lanthanum Bromide. *IEEE Trans. Nucl. Sci.* **2009**, *56*, 873–880. [CrossRef]
12. Seeley, Z.; Cherepy, N.; Payne, S. Homogeneity of Gd-based garnet transparent ceramic scintillators for gamma spectroscopy. *J. Cryst. Growth* **2013**, *379*, 79–83. [CrossRef]
13. Cherepy, N.; Payne, S.A.; Seeley, Z.; Cohen, P.C.; Andreaco, M.S.; Schmand, M.J. Transparent Ceramic Garnet Scintillator Detector for Positron Emission Tomography. U.S. Patent 10,000,698, 19 June 2018.
14. Nargelas, S.; Talochka, Y.; Vaitkevičius, A.; Dosovitskiy, G.; Buzanov, O.; Vasil'Ev, A.; Malinauskas, T.; Korzhik, M.; Tamulaitis, G. Influence of matrix composition and its fluctuations on excitation relaxation and emission spectrum of Ce ions in $(Gd_xY_{1-x})_3Al_2Ga_3O_{12}:Ce$ scintillators. *J. Lumin.* **2022**, *242*, 118590. [CrossRef]

15. Lecoq, P.; Morel, C.; O Prior, J.; Visvikis, D.; Gundacker, S.; Auffray, E.; Križan, P.; Turtos, R.M.; Thers, D.; Charbon, E.; et al. Roadmap toward the 10 ps time-of-flight PET challenge. *Phys. Med. Biol.* **2020**, *65*, 21RM01. [CrossRef] [PubMed]

16. Prusa, P.; Kamada, K.; Yoshikawa, A.; Kucera, M.; Nikl, M. *(Lu,Gd)$_3$(Al,Ga)$_5$O$_{12}$:Ce Scintillator—A Short History. XXXVI Days of Radiation Protection Book of Presentations and Posters*; International Nuclear Information System: Poprad, Slovakia, 2014; p. 1171.

17. Kamada, K.; Yoshikawa, A.; Endo, T.; Tsutsumi, K.; Shoji, Y.; Kurosawa, S.; Yokota, Y.; Prusa, P.; Nikl, M. Growth of 2-inch size Ce:doped Lu$_2$Gd$_1$Al$_2$Ga$_3$O$_{12}$:Ce single crystal by the Czochralski method and their scintillation properties. *J. Cryst. Growth* **2015**, *410*, 14–17. [CrossRef]

18. Witkiewicz-Lukaszek, S.; Gorbenko, V.; Zorenko, T.; Sidletskiy, O.; Gerasymov, I.; Fedorov, A.; Yoshikawa, A.; Mares, J.A.; Nikl, M.; Zorenko, Y. Development of composite Scintillators based on Single crystalline films and crystals of Ce^{3+} doped (Lu,Gd)$_3$(Al,Ga)$_5$O$_{12}$ mixed garnet compounds. *Cryst. Growth Des.* **2018**, *18*, 1834–1842. [CrossRef]

19. Chen, X.; Hu, Z.; Dai, J.; Chen, H.; Shi, Y.; Kou, H.; Kučerková, R.; Beitlerová, A.; Nikl, M.; Li, J. Fabrication and optical properties of Ce doped Lu$_3$Ga$_3$Al$_2$O$_{12}$ scintillation ceramics. *Opt. Mater.* **2018**, *85*, 121–126. [CrossRef]

20. Chewpraditkul, W.; Pattanaboonmee, N.; Chewpraditkul, W.; Kamada, K.; Yoshikawa, A.; Nikl, M. Luminescence and scintillation response of YGd$_2$Al$_2$Ga$_3$O$_{12}$:Ce and LuGd$_2$Al$_2$Ga$_3$O$_{12}$:Ce scintillators. *Radiat. Meas.* **2016**, *90*, 153–156. [CrossRef]

21. Chewpraditkul, W.; Pattanaboonmee, N.; Chewpraditkul, W.; Szczesniak, T.; Moszynski, M.; Kamada, K.; Yoshikawa, A.; Kucerkova, R.; Nikl, M. Optical and scintillation properties of LuGd$_2$Al$_2$Ga$_3$O$_{12}$:Ce, Lu$_2$GdAl$_2$Ga$_3$O$_{12}$:Ce, and Lu$_2$YAl$_2$Ga$_3$O$_{12}$:Ce single crystals: A comparative study. *Nucl. Instr. Methods Phys. Res. A* **2021**, *1004*, 165381. [CrossRef]

22. Glodo, J.; Wang, Y.; Shawgo, R.; Brecher, C.; Hawrami, R.H.; Tower, J.; Shah, K.S. New Developments in Scintillators for security Applications. *Phys. Porc.* **2017**, *90*, 285–290. [CrossRef]

23. Available online: https://www.dynasil.com/product-category/scintillators/scintillation-detectors/gamma-neutron-ceramic-scintillation-detector-glugag/ (accessed on 15 June 2022).

24. Babin, V.; Herman, P.; Kucera, M.; Nikl, M.; Zazubovich, S. Effect of Mg^{2+} co-doping on the photo- and thermally stimulated luminescence of the (Lu,Gd)3(Ga,Al)$_5$O$_{12}$:Ce epitaxial films. *J. Lumin.* **2019**, *215*, 116608. [CrossRef]

25. Lecoq, P.; Gektin, A.; Korzhik, M. *Inorganic Scintillators for Detector Systems: Physical Principles and Crystal Engineering*, 2nd ed.; Springer International Publishing: Berlin/Heidelberg, Germany, 2017.

26. Khanin, V.; Venevtsev, I.; Chernenko, K.; Pankratov, V.; Klementiev, K.; van Swieten, T.; van Bunningen, A.J.; Vrubel, I.; Shendrik, R.; Ronda, C.; et al. Exciton interaction with Ce^{3+} and Ce^{4+} ions in (LuGd)$_3$(Ga,Al)$_5$O$_{12}$ ceramics. *J. Lumin.* **2021**, *237*, 118150. [CrossRef]

27. Khanin, V.M.; Rodnyi, P.A.; Wieczorek, H.; Ronda, C.R. Electron Traps in Gd$_3$Ga$_3$Al$_2$O$_{12}$:Ce Garnets Doped with Rare-Earth Ions. *Tech. Phys. Lett.* **2017**, *43*, 439–442. [CrossRef]

28. Khanin, V.M.; Vrubel, I.I.; Polozkov, R.G.; Venevtsev, I.D.; Rodnyi, P.A.; Tukhvatulina, T.; Chernenko, K.; Drozdowski, W.; Witkowski, M.E.; Makowski, M.; et al. Complex Garnets: Microscopic Parameters Characterizing Afterglow. *J. Phys. Chem. C* **2019**, *123*, 22725–22734. [CrossRef]

29. Schauer, P.; Lalinský, O.; Kučera, M.; Lučeničová, Z.; Hanuš, M. Effect of Mg co-doping on cathodoluminescence properties of LuGAGG:Ce single crystalline garnet films. *Opt. Mater.* **2017**, *72*, 359–366. [CrossRef]

30. Rodnyi, P.A.; Venevtsev, I.D.; Khanin, V.M. Thermal quenching of luminescence in (Lu,Gd,Y)$_3$(Ga, Al)$_5$O$_{12}$:Ce complex garnet ceramics at high and low temperatures. *Phys. Complex Syst. Saint Petersburg Russia* **2021**, *2*, 1–5. [CrossRef]

31. Babin, V.; Chernenko, K.; Kučera, M.; Nikl, M.; Zazubovich, S. Photostimulated luminescence and defects creation processes in Ce- doped epitaxial films of multicomponent Lu$_{3-x}$Gd$_x$Ga$_y$Al$_{5-y}$O$_{12}$ garnets. *J. Lumin.* **2016**, *179*, 487–495. [CrossRef]

32. Korzhik, M.; Alenkov, V.; Buzanov, O.; Fedorov, A.; Dosovitskiy, G.; Grigorjeva, L.; Mechinsky, V.; Sokolov, P.; Tratsiak, Y.; Zolotarjovs, A.; et al. Nanoengineered Gd3Al2Ga3O12 scintillation materials with disordered garnet structure for novel detectors of ionizing radiation. *Cryst. Res. Technol.* **2019**, *54*, 1800172. [CrossRef]

33. Dosovitskiy, G.; Dubov, V.; Karpyuk, P.; Volkov, P.; Tamulaitis, G.; Borisevich, A.; Vaitkevičius, A.; Prikhodko, K.; Kutuzov, L.; Svetogorov, R.; et al. Activator segregation and micro-luminescence properties in GAGG: Ce ceramics. *J. Lumin.* **2021**, *236*, 118140. [CrossRef]

34. Gordienko, E.; Fedorov, A.; Radiuk, E.; Mechinsky, V.; Dosovitskiy, G.; Vashchenkova, E.; Kuznetsova, D.; Retivov, V.; Korjik, M.; Sandu, R. Synthesis of crystalline Ce-activated garnet phosphor powders and technique to characterize their scintillation light yield. *Opt. Mater.* **2018**, *78*, 312–318. [CrossRef]

35. Auffray, E.; Augulis, R.; Fedorov, A.; Dosovitskiy, G.; Grigorjeva, L.; Gulbinas, V.; Koschan, M.; Lucchini, M.; Melcher, C.; Nargelas, S.; et al. Excitation Transfer Engineering in Ce-Doped Oxide Crystalline Scintillators by Codoping with Alkali-Earth Ions. *Phys. Stat. Sol.* **2018**, *215*, 1700798–1700808. [CrossRef]

36. Dosovitskiy, G.; Fedorov, A.; Mechinsky, V.; Borisevich, A.; Tret'Jak, E.; Korjik, M. Persistent luminescence in powdered and ceramic polycrystalline Gd$_3$Al$_2$Ga$_3$O$_{12}$:Ce. *IOP Conf. Ser. Mater. Sci. Eng.* **2017**, *169*, 012014. [CrossRef]

37. Yokota, M.; Tanimoto, O. Effects of Diffusion on Energy Transfer by Resonance. *J. Phys. Soc. Jpn.* **1967**, *22*, 779–784. [CrossRef]

38. Weber, M.J. Multiphonon Relaxation of Rare-Earth Ions in Yttrium Orthoaluminate. *Phys. Rev. B* **1973**, *8*, 54–64. [CrossRef]

39. Momma, K.; Izumi, F. VESTA 3 for three-dimensional visualization of crystal, volumetric and morphology data. *J. Appl. Cryst.* **2011**, *44*, 1272–1276. [CrossRef]

40. Onderisinova, Z.; Kucera, M.; Hanus, M.; Nikl, M. Temperature-dependent nonradiative energy transfer from Gd^{3+} to Ce^{3+} ions in co-doped LuAG:Ce,Gd garnet scintillators. *J. Lumin.* **2015**, *167*, 106–113. [CrossRef]

41. De Vries, A.J.; Kiliaan, H.S.; Blasse, G. An investigation of energy migration in luminescent diluted Gd^{3+} system. *J. Solid State Chem.* **1986**, *65*, 190–198. [CrossRef]
42. Barandiarán, Z.; Seijo, L. Quantum chemical analysis of the bond lengths in f^n and $f^{n-1}d^1$ states of Ce^{3+}, Pr^{3+}, Pa^{4+}, and U^{4+} defects in chloride hosts. *J. Chem. Phys.* **2003**, *119*, 3785–3790. [CrossRef]
43. Setlur, A.A.; Shiang, J.J.; Vess, C.J. Transition from Long-Range to Short-Range Energy Transfer through Donor Migration in Garnet Hosts. *J. Phys. Chem. C* **2011**, *115*, 3475–3480. [CrossRef]
44. Omelkov, S.; Kirm, M.; Pustovarov, V.; Isaenko, L. Energy transfer in pure and rare-earth doped SrAlF5 crystals. *IOP Conf. Ser. Mater. Sci. Eng.* **2010**, *15*, 012011. [CrossRef]
45. Tikhonov, A.N. Solution of incorrectly formulated problems and the regularization method. *Sov. Math.* **1963**, *4*, 1035–1038.
46. Korzhik, M.; Tamulaitis, G.; Vasil'ev, A.N. *Physics of Fast Processes in Scintillators*; Springer International Publishing: Cham, Switzerland, 2020; Chapter 5.7.
47. Kanai, T.; Satoh, M.; Miura, I. Characteristics of a Nonstoichiometric $Gd_{3+\delta}(Al,Ga)_{5-\delta}O_{12}$:Ce Garnet Scintillator. *J. Am. Ceram. Soc.* **2008**, *91*, 456–462. [CrossRef]
48. Liu, S.; Mares, J.A.; Babin, V.; Hu, C.; Kou, H.; D'Ambrosio, C.; Li, J.; Pan, Y.; N Nikl, M. Composition and properties tailoring in Mg^{2+}codoped non-stoichiometric LuAG:Ce,Mg scintillation ceramics. *J. Eur. Ceram. Soc.* **2017**, *37*, 1689–1694. [CrossRef]
49. Korzhik, M.V. *Physics of Scintillators on a Base of Oxide Single Crystals*; BSU: Minsk, Belarus, 2003; p. 263. ISBN 985-485-061-7.
50. Belsky, A.N.; Auffray, E.; Lecoq, P.; Dujardin, C.; Garnier, N.; Candibano, H.; Pedrini, C.; Petrosyan, A.G. Progress in the development of LuAlO3-based scintillators. *IEEE Trans. Nucl. Sci.* **2001**, *48*, 1095–1100. [CrossRef]